Available online at www.sciencedirect.com
SCIENCE DIRECT®
Journal of Sound and Vibration 276 (2004) 649–669
JOURNAL OF SOUND AND VIBRATION
www.elsevier.com/locate/jsvi

Development and evaluation of a 3-D microphone array to locate individual acoustic sources in a high-speed jet

J. Hileman, B. Thurow, M. Samimy*

Gas Dynamics and Turbulence Laboratory, Department of Mechanical Engineering, The Ohio State University, 206 West 18th Avenue, Columbus, OH 43210-1107, USA

Received 7 October 2002; accepted 4 August 2003

Abstract

A 3-D microphone array was developed, evaluated, and used to locate the origins of individual sound waves that were created within a high-speed, high Reynolds number, turbulent jet. In previous work by the authors, a linear array of microphones and simultaneous temporally resolved flow visualizations were used to determine the origin of individual sound waves and their generation mechanisms within the jet. The linear array algorithm assumed the noise sources were distributed along the jet axis, and was not able to resolve off-axis locations of noise sources. Further, the registration of sound radiation from similar phenomena within the mixing layer was observed to depend on whether the phenomena occurred on the array side of the jet or the opposite side. Based on these error sources and observations, a new array was developed that can locate the individual sources of sound waves within three dimensions. This work presents the development of this array, its validation, and its use to locate noise sources within a high-speed jet. The 3-D array with its accompanying noise source location algorithm is quite robust and accurate as it predicted the precise location of noise sources from a plasma arc, a high-frequency fluidic device, and the expected radial distribution of noise sources from a high-speed jet.

1. Introduction

This work presents progress on research being conducted on the acoustics of axisymmetric high-speed jets. The purpose of the overall research project is to relate the development and interaction of large-scale turbulence structures within the jet's mixing layer to radiated farfield noise. Noise generation mechanisms are being determined by comparing the origin of individual sound 'events' to simultaneously acquired real-time flow visualization using advanced laser-based

*Corresponding author. Tel.: +1-614-292-6988; fax: +1-614-292-3163.
E-mail address: samimy.1@osu.edu (M. Samimy).

0022-460X/$ - see front matter © 2003 Elsevier Ltd. All rights reserved.
doi:10.1016/j.jsv.2003.08.022

optical diagnostics. The specific purpose of this work is to present the development and use of a microphone array that can locate the origin of individual sound events in three-dimensional space. Some of the pertinent results from previous work [1,2] will be briefly reviewed in this introduction as well as other work that directly relate to the development of the array.

The farfield noise for a Mach 1.3 jet, which is the focus of this research program, is most intense at an angle of 30° with respect to the downstream jet axis at a frequency of about 3 kHz ($St_D = 0.2$) [1]. It is known that large-scale turbulence structures generate this intense noise. Since the overall goal of the current research is to explore the correlation between these structures and the radiated farfield noise, an inline array of four microphones was placed at this orientation in the far field to determine where this sound was being created [2]. The origin of individual acoustic events was determined using the phase lag between individual microphones recording the sound wave of interest and the relative locations of the microphone and nozzle. The origin for every event that had a magnitude in excess of 1.5 times the standard deviation of the overall measured sound pressure was resolved. The majority (74%) of the sound, regardless of its frequency content, was created between 4 and 9 jet diameters [2]. Other researchers, using various techniques, have determined that the mean source locations for acoustic radiation between St_D of 0.1 and 1.0 were between $4x/D$ and $13x/D$, which is the region including and surrounding the end of the potential core of the jet [3–11]. By utilizing various microphone arrays, several research groups have found that the high-frequency noise from high subsonic jets is generated near the nozzle exit, while lower-frequency noise originates farther downstream [7–11].

There were a number of issues with the inline microphone array used in Ref. [1,2]. One of the underlying assumptions was that the noise sources were distributed along the jet centerline. As discussed in Ref. [1], the assumption of a centerline distribution of noise sources added 0.9 jet diameters (23 mm) uncertainty to the overall error in the streamwise noise source location for a dual microphone array (this assumed an uncertainty of $\pm 0.5D$ in radial distance). Many of the dimensions in this work will be non-dimensionalized by the jet diameter, D, which is 25.4 mm. Another cause of concern, which was raised in Ref. [2], was that on occasion a structure roll-up within the top half of the mixing layer (the side where the array was located) corresponded with intense noise emission within the ceiling mounted array while an equivalent structure roll-up within the bottom half of the mixing layer did not. This observation raised the question of whether this difference was due to sound wave refraction within the jet or due to asymmetric radiation. If a sound wave were generated within the bottom half of the mixing layer, then it would have to travel through the core of the jet and the opposite half of the mixing layer before radiating to the ceiling mounted microphones. The trajectory of such a wave would be drastically modified as was shown in Ref. [12], which explored acoustic refraction in a jet using direct numerical simulation. Unfortunately, an inline array mounted on one side of the jet is not capable of resolving such issues.

Based on these inherent problems using an inline array to determine instantaneous noise source locations within a high-speed jet, a microphone array was developed that could identify the origin of individual sound events in three-dimensional space. This paper discusses the development, evaluation, and application of such an array. The remainder of this paper can be divided into three parts: (1) the development of a 3-D microphone array with inline and azimuthally distributed elements, (2) the validation of the array using known noise sources, and (3) a

presentation and discussion of the use of this array for the determination of the noise emitting region in high-speed jets.

2. The 3-D array

2.1. Design of the array

To measure noise source origins in three dimensions, one has to have a distribution of microphones in space. With an inline array, only a linear distribution of noise sources can be resolved. An azimuthal distribution of microphones would be able to determine the noise source locations azimuthally, but not axially. If this azimuthal array is used in conjunction with an inline array that is normal to the plane of the azimuthal array, then the three components of the noise source location can be determined. Therefore, both an azimuthal and a linear distribution of microphones were used to resolve the instantaneous location of the noise sources in three dimensions.

To monitor the entire jet, the azimuthal distribution of microphones needs to encompass as large an area as possible without significant loss of sound wave coherence. To determine what this separation should be, the coherence level between the radiated sound that was recorded at different azimuthal microphone separations was measured. Coherence values were obtained between microphones placed in the acoustic far field at an angle of 30° with respect to the jet axis (downstream distance of 61.5D and radial distance of 38.5D). These coherence levels were averaged over frequencies between 1 and 10 kHz to yield the upper curve presented in Fig. 1. The choice of this frequency range came from our earlier results that showed the broadband peak

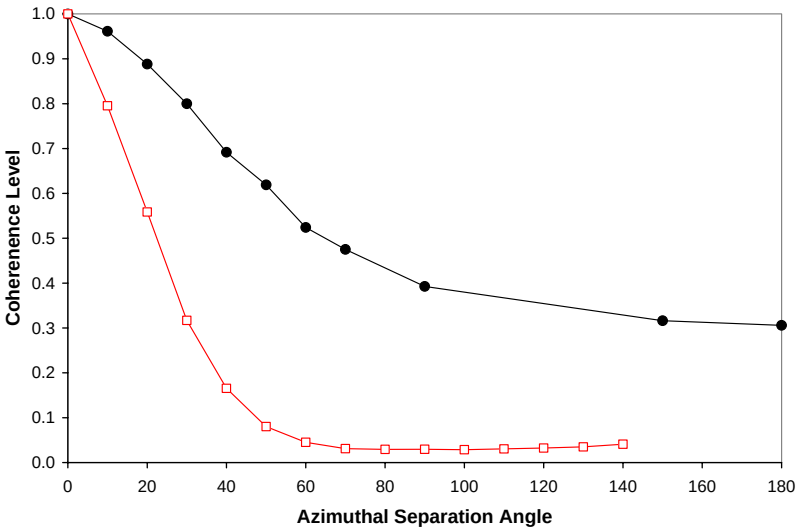

Fig. 1. Coherence levels in the acoustic far field at two polar angles (30° and 60°, with respect to the downstream axis) for various azimuthal microphone separations (frequency band of 1–10 kHz). The 30° data are marked by solid circles while the open squares show the 60° data.

frequency at 30° is between 2 and 4 kHz [1]. Since the coherence level is quite high for the 60° azimuthal separation (over 0.5), and there were eight microphones available for the array, six equally spaced azimuthal locations were chosen for the configuration. As shown in Fig. 2, three of the microphones were on the top-half (microphones 1, 2 and 4) and three were on the bottom-half (microphones 5, 6 and 8). At the top (0°) and bottom (180°) microphone locations, a second microphone was placed 7.5D (19.1 cm) behind the front microphone (microphones 3 and 7). The rest of this paper uses the conventions of this figure. The lower curve presented in Fig. 1 shows the average coherence value between 1 and 10 kHz for an angle of 60° with respect to the jet axis (downstream distance of 14.8D and radial distance of 26.0D). As expected, the coherence at the 60° location is significantly lower than the 30° location for all azimuthal separations.

The effect of streamwise microphone spacing on coherence is shown in the curves of Fig. 3. Again, the ordinate shows the average coherence over a frequency range of 1–10 kHz, while the abscissa gives the downstream separation between the two microphones. For the 90° curve, a microphone was fixed below the nozzle exit; while for the 30° curve, the first microphone was fixed at a downstream location of 45 jet diameters. For both curves, the radial distance of the microphones was 26 jet diameters. The separation distances for the 90° curve correspond to angles between 90.0° and 66.1°; while those of the 30° curve coincide with angles between 30.0° and 24.7°. The coherence level for a 7.5 jet diameter spacing at 30° was above 0.7 justifying the use of this spacing in the array design. Furthermore, such a large spacing between inline microphones has been used in previous arrays without any problem [1,2].

The difference in the coherence levels observed for downstream locations of 30° and those at 60° or 90° is due to the source of the sound emission. The relatively high coherence between microphones at a downstream location of 30° (as measured in either the downstream or azimuthal directions) can be attributed to the radiation of sound from dynamics of larger turbulence structures. The other two downstream locations have dramatically lower coherence between microphones at comparable separations, and this corresponds to sound radiation from dynamics of smaller turbulence scales. These results are in agreement with the results presented in Ref. [1], showing that the acoustic spectra for 60° and 90° are flat between 1 and 10 kHz; whereas there is a large, broad peak for these frequencies at 30°. Also in agreement with these results, in Ref. [13], an

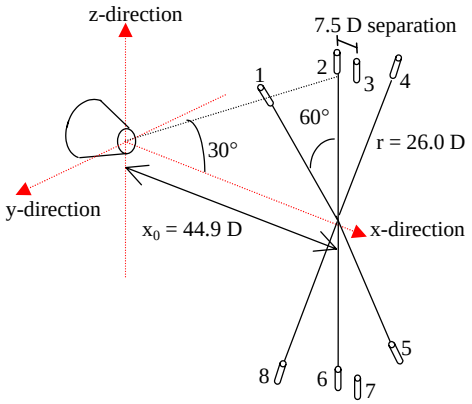

Fig. 2. Schematic of the microphone locations in the 3-D array relative to the nozzle exit and jet axis.

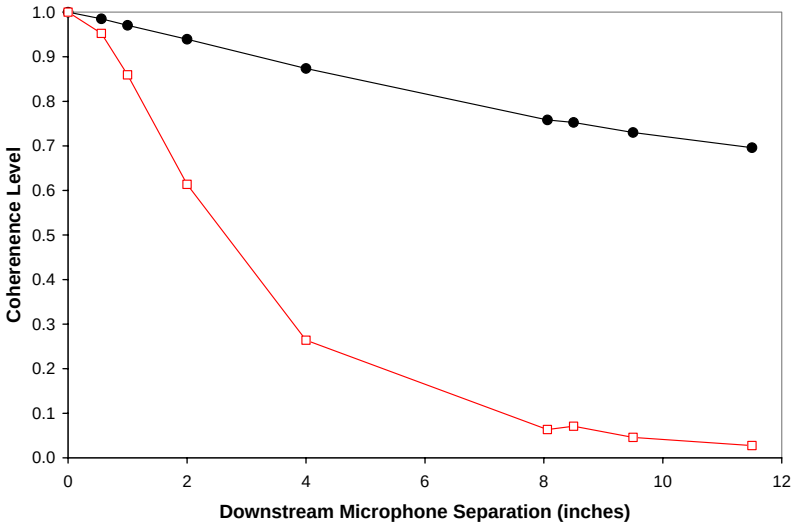

Fig. 3. Coherence levels in the acoustic far field at two polar angles (30° and 90°, with respect to the downstream axis) for various downstream microphone separations (frequency band of 1–10 kHz). The 30° data are marked by solid circles while the open squares show the 90° data.

ensemble averaged acoustic waveform shows a short time scale for 60° and 90°, but a much larger scale for 30°. Since our goal is to create a microphone array for the analysis of sound emission from the largest structures within a high-speed jet, and the characteristics of the sound emission match those from large coherent structures at an array location of 30°, this location was chosen for the analysis.

The backbone of the 3-D array is a 2.54 cm thick aluminum ring that has an inner diameter of 1.52 m and an outer diameter of 1.68 m. The inner diameter was held to a tolerance of 0.25 mm. Pairs of holes (radial separation of 5.08 cm) were drilled around the periphery of the ring at 10° azimuthal increments as well as the multiples of 45° to allow for other microphone configurations. The array is mounted to the floor and ceiling of the anechoic chamber via the top and bottom sets of holes within the aluminum ring. Guide wires connected to the walls of the anechoic chamber hold the sides of the array fixed. The hole sets were designed to facilitate custom-built, precision microphone mounts that held a single microphone at a fixed distance from the inner radius of the ring. The distance from the inside of the ring to the diaphragm of the microphone could be precisely measured and fixed by a set screw. Therefore, the distance from the microphone to the jet centerline was controlled by how accurately the ring could be centered on the jet centerline. The inline microphones were housed in aluminum blocks that were attached to the mounting brackets at the top and bottom of the ring. The height of the pedestals used in the azimuthal mounts was selected to match the distance from the front microphone of the inline array to the front of the ring. Hence, all six azimuthally distributed microphones were at the same downstream location relative to the front of the ring, and the position of all eight microphones was determined by the ring placement. Fig. 4 shows a photograph of the arc array within the anechoic chamber. During data acquisition, the array would be wrapped in acoustic foam.

Fig. 4. Photograph of the arc array in the anechoic chamber. For actual data acquisition, the ring was wrapped in acoustic foam.

2.2. Noise location algorithm

The principles behind the 3-D array are the same as those used in the aforementioned inline array [1,2]. In those works, the delay between when a sound 'event' passed two microphones (phase lag) was used to determine the noise source location within the jet. With the delay and the knowledge of the geometry of the experiment, the flight path of the wave along the direction of the microphones was determined [1,2]. The same principle is now being extended to microphones in three-dimensional space.

The first step in the noise source location algorithm was to identify sound 'events' that are of interest. The sound data was normalized by its standard deviation. Fig. 5 shows the acoustic time trace from the top two inline microphones of the array for a random data set. Several peaks have been marked with either a '1' or '2' denoting the microphone that recorded them. The acoustic peaks that had a magnitude above 1.5 are referred to as acoustic 'events,' and the time of their relative maxima was recorded. The acoustic time trace from the front inline microphones were used to determine the acoustic events of interest.

The time delay was determined by finding the maximum value of the correlation coefficient, ρ_{ab}, between two microphone signals, a and b. The correlation coefficient is given by

$$\rho_{ab}(\tau) = \frac{\langle a(t)b(t+\tau)\rangle - \mu_a\mu_b}{\sigma_a\sigma_b}, \tag{1}$$

where $\langle\ \rangle$ is the time average, τ is a time delay, σ is the standard deviation, and μ is the mean. The correlation coefficient is only computed over a range of values of τ that are realistic, i.e., those delays that would be expected if the sound had originated within the jet. The signal length chosen

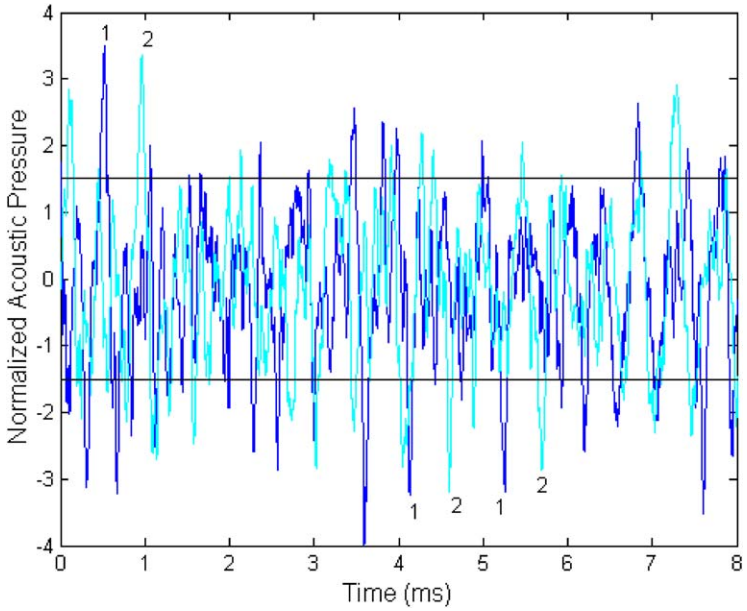

Fig. 5. Acoustic time signatures from the top inline microphones; amplitude is normalized by the standard deviation.

for correlation was 350 μs. This length was chosen since it would contain a single sound pressure peak (the frequency of the jet noise was broadband and centered between 2 and 4 kHz).

An algorithm was developed that could take the time delays and then determine where the noise source was located. After some exploration, it was decided to use the microphone location vectors, $\vec{M} = [x_m, y_m, z_m]$, in conjunction with an iterative routine to determine the apparent noise source location, $\vec{S} = [x_s, y_s, z_s]$. The jet exit center is set as the origin. If the location of a noise source were known, then the time delay between a sound wave reaching two microphones 'i' and 'j', Δt_{ij}, could be determined by the following vector equation:

$$\Delta t_{ij} = t_i - t_j = \frac{|\vec{M}_i - \vec{S}| - |\vec{M}_j - \vec{S}|}{c}, \tag{2}$$

where t_i is the time microphone 'i' recorded the peak of the sound wave, $\vec{M}_i$ is the vector location of microphone 'i,' $\vec{M}_j$ is the vector location of microphone 'j,' c is the ambient speed of sound, and $|\bullet|$ is the norm of a vector. Since Δt_{ij} is known, but $\vec{S}$ is not, the appropriate approach is to find what value of $\vec{S}$ causes Q_{dummy} to be equal to zero in the equation

$$Q_{dummy} = \frac{|\vec{M}_i - \vec{S}| - |\vec{M}_j - \vec{S}|}{c} - \Delta t_{ij}. \tag{3}$$

An initial value for $\vec{S}$ is assumed for the noise source with one of the components varied to find what value will render Q_{dummy} equal to zero. If the value of the component returned from this procedure was infinity or not a number, then the previous value was used instead. Now that the procedure of finding the noise source location from a time separation has been determined, the next question is, "which microphone pairs (i–j) should be used to determine the source location?"

The azimuthally distributed microphones have to be used to determine the y- and z-components of the noise source (see Fig. 2 for the coordinate system used). The iterative routine starts with the determination of the z-component, and later that value is used to compute the y-component. The best choice of microphone pairs for the z-component would be those microphones that straddle the $y = 0$ plane. Thus, microphone pairs 4, 5 and 1, 8 are used. Eq. (3) is first used with i equal to 4 and j equal to 5 to determine a value for the z-component. This is then repeated with i equal to 1 and j equal to 8 to determine another value for the z-component. In both cases, the initial guess for $\vec{S}$ was $[0, 0, 0]$. The two values for the z-component are then averaged to get the first iteration value for z_s.

The determination of the x- and y-component of $\vec{S}$ relies on a pre-existing knowledge of the z-location (vertical) of the noise source. This is due to the previously described refraction effect. The most accurate measure of the flight path will be on the side of the jet mixing layer that contains the noise source. The z-component result from the previous paragraph could be used for this purpose, but there is a more accurate method. Instead, the time delay between opposite inline microphones is utilized. If the time delay between the front, inline microphones, Δt_{26}, is negative, then the sound wave of interest reached the top microphone before the bottom and the sound originated above the jet centerline. As a check of Δt_{26}, the time delay between the rear, inline microphones, Δt_{37}, is also determined. If both Δt_{26} and Δt_{37} are negative, then the source of the sound was above the jet centerline. The opposite case also holds. Refraction should be beneficial in this regard since any wave that is refracted will take longer to reach its destination than would a wave that was not refracted. Hence, the delay between a refracted wave reaching one microphone and the unrefracted wave leaving the opposite side toward the opposite microphone would be even larger than if neither wave had been refracted. If Δt_{26} and Δt_{37} do not have the same sign, then the previously computed value of z_s is used to determine which side of the jet contained the noise source.

The only way to determine x_s is to use the time delay between the inline microphones. Let us assume the analysis of the previous paragraph predicted the noise source was located above the jet centerline. In this case, the top set of inline microphones would be used to determine the x-component of the noise source location. Eq. (3) is then used with an initial guess of $[0, 0, z_s]$ for $\vec{S}$, and i and j are set, respectively, to 3 and 2. If the noise source was below the jet centerline, i and j would be set, respectively, to 7 and 6. In either case, the result is the value for the first iteration of x_s.

The y-component of the noise source is determined based on the microphone pairs that straddle the $z = 0$ plane. Unlike the z-component equations, there are three microphones on both the top and bottom of the ring that meet this requirement. Along the top of the ring, these pairs are 4, 2 and 1, 2; on the bottom, they are 5, 6 and 8, 6. Which pair is used depends on whether the noise source is above or below the jet centerline (this determination is the same as that used in the above x-component computations). If the noise source were determined to be above the jet centerline, Eq. (3) would be used with an initial guess for $\vec{S}$ of $[x_s, 0, z_s]$ and the values of i and j would be 4 and 2 to get one value for the y-component, and then this is repeated with i and j equal to 1 and 2. These two y-components are then averaged to get y_s. If the noise source were below the jet centerline, then the microphone values for i and j would be 5 and 6 for the one pair and 8 and 6 for the other pair. With the value for y_s the first iteration is complete.

After the first iteration is complete, a second iteration is automatically started. The coordinates for $\vec{S}$ from the first iteration are used as the initial guess for the second iteration. Additional iterations are performed with the value of $\vec{S}$ from the previous iteration as the new initial guess until the difference between subsequent values for all three co-ordinates are less than 0.1%. If the routine reaches a set number of iterations without convergence, then the location for that sound pressure peak was discarded.

2.3. Error analysis

A simple error analysis was conducted to assess a worst-case estimate of the uncertainty. The error sources were broken up in the following categories: (1) accuracy in the microphone placement relative to the ring structure, changes in the ambient conditions within the anechoic chamber, and accuracy in the measurement of the time delays; (2) accuracy in the placement of the ring structure with respect to the jet centerline and nozzle exit; (3) other uncertainties that can only be speculated upon at this point.

The sources within the first two listed items are discussed in detail within Appendix A. Each of the uncertainties was varied to yield a worst-case scenario that gave a maximum deviation for a set of time delays. Based on that simplified analysis, the uncertainty in the streamwise direction (x-component) for this array would be about 25 mm while the uncertainties in the y- and z-component would be negligible.

These values are a vast improvement over the estimated uncertainties for the linear arrays used in Refs. [1,2]. The dual element array of Ref. [1] had an estimated worst-case uncertainty in the streamwise location of ± 65 mm. The four-element inline array of Ref. [2] had an estimated worst-case uncertainty of ± 50 mm in the noise source location, but it located a noise source to within a ± 13 mm range. A large portion of the estimated uncertainty for both of these inline arrays came from the centerline assumption, which has been eliminated with the present configuration.

As mentioned in item 3, there are also other sources of uncertainty with less known nature and extent. These sources include distributed source effects, source convection effects, and the effect of refraction on the sound wave trajectory. The analysis of Ref. [14] can be used to show that the effect of noise convection is insignificant. The effects of a distributed source are covered in the validation of the array in Section 3 and an analysis for the effects of refraction and source convection is presented in Ref. [14]. Refraction will undoubtedly affect the flight path of a sound wave as it travels through the mixing layer of the jet. This error source is minimized by first determining which side of the jet contained the noise source, and then using microphones that are on that side of the jet to compute the x- and y-component of the noise source.

2.4. Microphone equipment

The microphones used in the experiments were either Bruel & Kjaer 4135 or 4939 0.635 mm (1/4 in) condenser microphones connected to Bruel & Kjaer 2670 preamplifiers. The data from the microphones passed through two Bruel & Kjaer Nexus conditioning amplifiers before being recorded by a pair of National Instruments PC-6110E data acquisition boards at a rate of 1 MHz. The two boards were synchronized via an internal RTSI connection.

2.5. Anechoic chamber

The optically accessed anechoic chamber of the Gas Dynamics and Turbulence Laboratory was used to conduct the array experiments. The chamber was tested for compliance to ANSI Standard S12.3535, and the results from the tests were within the required tolerance over most of the distances along the microphone paths [15]. The inner dimensions of the chamber measure, from wedge tip to wedge tip, 3.1 m in width and length, and 2.7 m in height. Additional details of the anechoic chamber and jet flow facility can be found in Refs. [1,2,15].

3. Validation of the array

Two different noise generators were used to test the ability of the array to locate noise sources. The first was a plasma (spark) generated between a pair of wires at varying frequency. The other was a Hartmann tube fluidic actuator (HTFA) [16,17], which is also referred to as a powered resonance tube in the literature [18]. The sound from the plasma was approximately a point source, more precisely a short line source (the stationary arc), while that from the HTFA was distributed over a small area of moving fluid. Additionally, a simple simulation was performed to determine the ability of the array to locate a distributed noise source.

The plasma arc was created by applying a sinusoidal voltage of 15 kV across a small gap of 3 mm ($0.1D$) between two electrodes. By varying the input sine wave, the frequency with which the arc fired varied from 1 to 20 kHz. With this variation, the plasma arc was also used to analyze the ability of the array to locate noise sources of varying frequency. The plasma arc was located at a location of $[x/D, y/D, z/D] = [8, 0, 0]$ in all of these experiments. For each case, at least 0.15 s of data were analyzed, which yielded thousands of individual noise source locations for each of the frequencies. Figs. 6–8 show the average and standard deviations for the three spatial coordinates of the calculated noise source locations. Since the source is a stationary point, there should be minimal deviation among the calculated sound origins. The standard deviation of the x-component of the noise source location deviates from zero above 10 kHz, the z-component above 12 kHz, and the y-component above 14 kHz. These also match the frequencies where the means deviate from the actual plasma location (these are marked by the horizontal lines in the three figures). Based on these results, the array is capable of accurately locating noise sources with frequency content up to 10 kHz. Therefore, the upper end of the operation range of this array configuration is 10 kHz.

For frequencies of 3 and 12 kHz, the plasma arc was precisely located with respect to the nozzle exit. The desired location was measured to within approximately 1 mm of the center of the jet nozzle exit, and then two lasers were used to mark this point in space. The electrodes that were used to create the plasma arc were placed to straddle the two laser beams. For the lower frequency (3 kHz), the mean of the calculated noise origins was $[x/D, y/D, z/D] = [8.17, 0.02, 0.18]$, while for the higher frequency (12 kHz) the mean was $[x/D, y/D, z/D] = [8.50, 0.01, 0.16]$. The x-component was expected to be in error for the higher frequency as this is beyond the resolvable frequency for the array and the y-component deviation is acceptable. The offset in the z-component likely originates within the array setup.

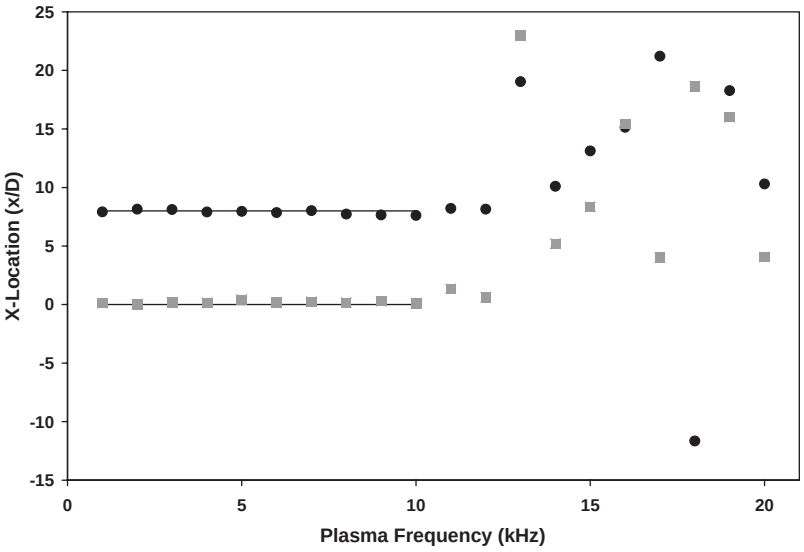

Fig. 6. Average noise source locations (x-component) for the plasma arc for various source frequencies. The average values are marked by the circles while the standard deviation values are shown with squares.

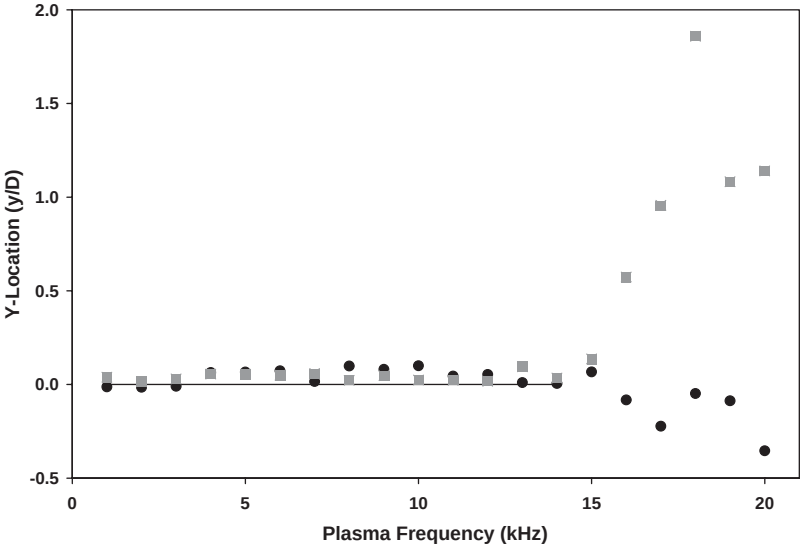

Fig. 7. Average noise source locations (y-component) for the plasma arc for various source frequencies. The average values are marked by the circles while the standard deviation values are shown with squares.

The most likely explanation for the small discrepancy in the z direction is that the center of the array was offset from the centerline of the jet by a small distance. The 3-D array projects noise sources onto a set of orthogonal coordinates where the x-co-ordinate passes through the center of, and is perpendicular to, the plane that is formed by the azimuthal distribution of microphones. If the center of the ring were offset from the center of the nozzle, then there would be an equal offset

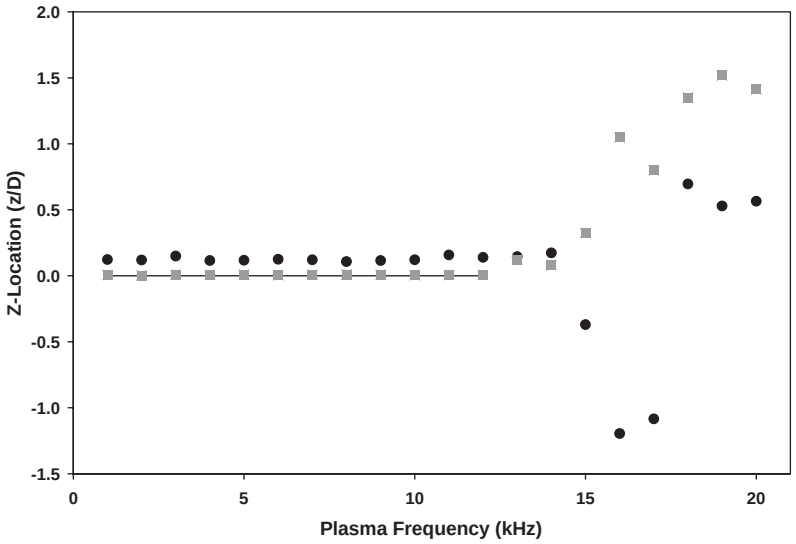

Fig. 8. Average noise source locations (z-component) for the plasma arc for various source frequencies. The average values are marked by the circles while the standard deviation values are shown with squares.

in the location of each noise source location from the jet centerline. An error of 5 mm ($0.2x/D$) should not be surprising for such a large array configuration. The positions of the microphones were modified within the noise processing codes by 5 mm in the negative z direction to eliminate this bias. The initial setup of the 3-D array, which was reported in Ref. [19], had a correction of -4.3 mm in the y direction and -7.1 mm in the z direction.

An HTFA was then used as a test of the array's ability to locate flow-induced acoustic sources. A Hartmann tube consists of an underexpanded jet and a closed-ended tube where the open end of the tube is placed within a compression region of the underexpanded jet [20]. An HTFA is created by placing a cylindrical shield between the nozzle and the tube that covers a large portion of the open area [16]. The HTFA used for the validation is based on the design described in Ref. [16] and was operated at a jet Mach number of 1.1. The converging nozzle of the HTFA had an exit diameter of 6 mm and the opening of the HTFA was square with 8 mm sides. By varying the length of the tube, the resonant frequency of the HTFA could be varied. Three tube lengths were used for the current validation. Two of the tubes created a pure tone, either 2.1 or 3.4 kHz; while the third tube created broadband acoustic radiation centered on 7 kHz. The spectra for the three cases, as well as the Mach 1.3 jet, are given in Fig. 9. All of these spectra were taken from the same microphone of the 3-D array. The opening of the HTFA was $4.9D$ downstream of the origin, centered on the nozzle exit plane, with air exiting the HTFA along the jet centerline.

All of the noise events exceeding 1.5 times the standard deviation were examined to determine the origin of the acoustic radiation for the three cases. The aforementioned z-component correction was applied to the microphone locations prior to processing. The probability density distributions in the x direction for all three cases have been plotted in Fig. 10. The majority of the noise sources were located within a 60 mm region. The distributions do vary slightly; the non-resonant case (7 kHz broad band) is distributed between $4x/D$ and $6.5x/D$ while the two tonal cases are between about $5x/D$ and $7x/D$. These distributions can be compared to the flow

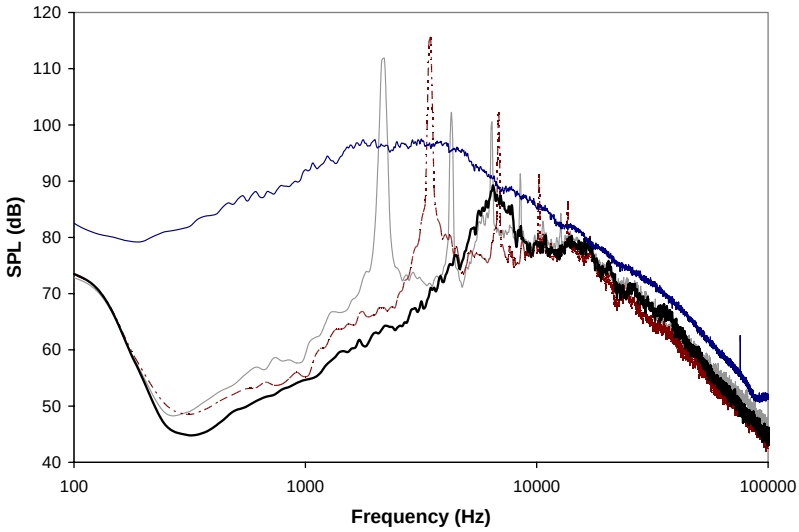

Fig. 9. HTFA spectra for the three geometries used along with the Mach 1.3 jet spectrum. Measurements are from the same array microphone. The 2.1 kHz tonal HTFA data are marked with a thin grey line, the 3.4 kHz tonal HTFA data are marked with a dotted line, the 7 kHz broadband HTFA data are marked with a thick black line, and the Mach 1.3 data are marked by a thin black line.

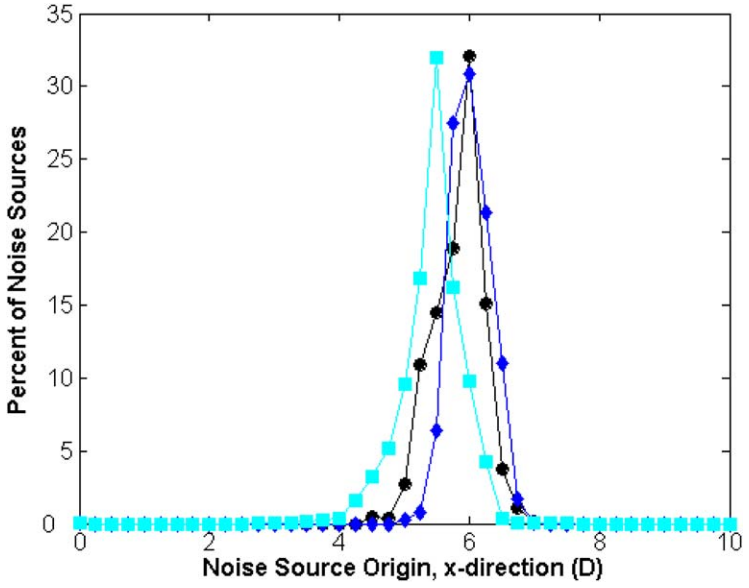

Fig. 10. Probability density distributions for the x-component of the noise source locations for the three HTFA cases. The 2.1 kHz tonal HTFA data are marked with circles, the 3.4 kHz tonal HTFA data are marked with diamonds, and the 7 kHz broadband HTFA data are marked with squares.

visualization images of Ref. [17], which shows the vortical structures emanating from the same 3.4 kHz, tonal HTFA that was used here. Ref. [16] also shows images from the HTFA used here, but it was being operated at a higher jet Mach number than was used here (1.3 instead of 1.1).

These two operating conditions produce vortical structures of similar shape, but they differ in length scales. For the jet Mach number used here, the flow images of Ref. [17] showed significant vortical flow activity over a range extending from the HTFA exit to past the end of the flow images at 50 mm. The most intense vortical activity occurred at the top of the images corresponding to a location of 50 mm, which is also the center of the 3.4 kHz, tonal noise distribution of Fig. 10.

The cross-stream distributions are given in the forms of 2-D probability density plots in Figs. 11–13 that cover a range of $0.5D$ (12.7 mm). The bin size is $0.05D$ in both directions. All three figures show distributions that are within $0.1D$ of the z-axis, but have an offset in the negative y direction. This offset matches the location of the edge of the HTFA opening where the flow images of Ref. [17] showed significant vortical flow. Hence, the area of noise generation again matches the area of maximum vortical activity.

To test the ability of the array to determine the origin of a distributed noise source, a simple computer simulation was performed. In the model, two monopole sound sources were located a fixed distance apart. The monopoles were located on the jet centerline, and their midpoint was initially at $9x/D$. The monopoles created in-phase, 3 kHz acoustic radiation. Hence, the model was of a distributed source of varying length. The time-varying acoustic radiation from such a source was then calculated for each of the array microphones using

$$p(t) = \frac{1}{r}\,\mathrm{Re}(A\mathrm{e}^{-\mathrm{i}\omega t}\mathrm{e}^{\mathrm{i}kr}), \tag{4}$$

where p is the pressure at the microphone, r is the distance between source and microphone, A is amplitude, ω is the angular frequency, and k is the wave number. The microphone array codes were then used to estimate the source of all acoustic waves for each source distribution. The

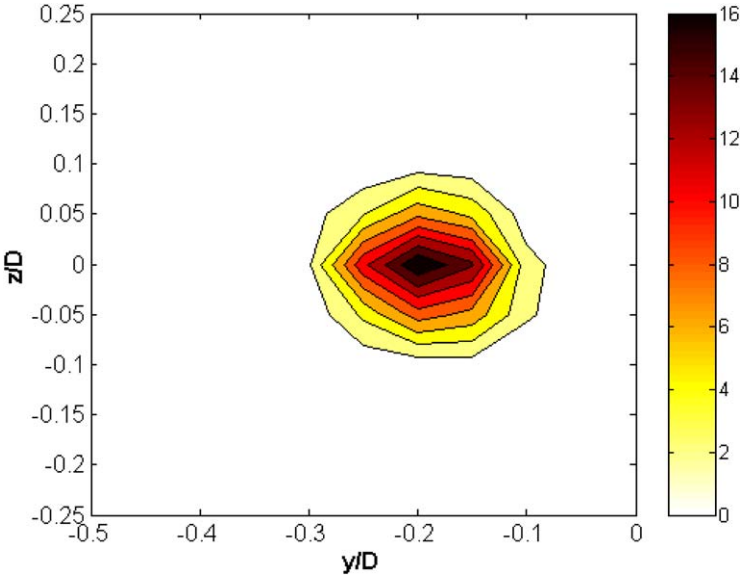

Fig. 11. Two-dimensional probability density distribution for the y- and z-component of the noise source locations for the 2.1 kHz tonal HTFA.

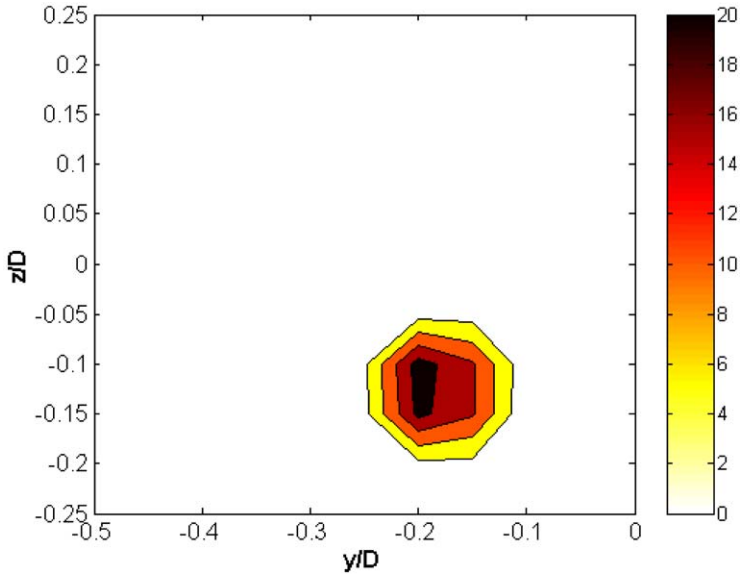

Fig. 12. Two-dimensional probability density distribution for the y- and z-component of the noise source locations for the 3.4 kHz tonal HTFA.

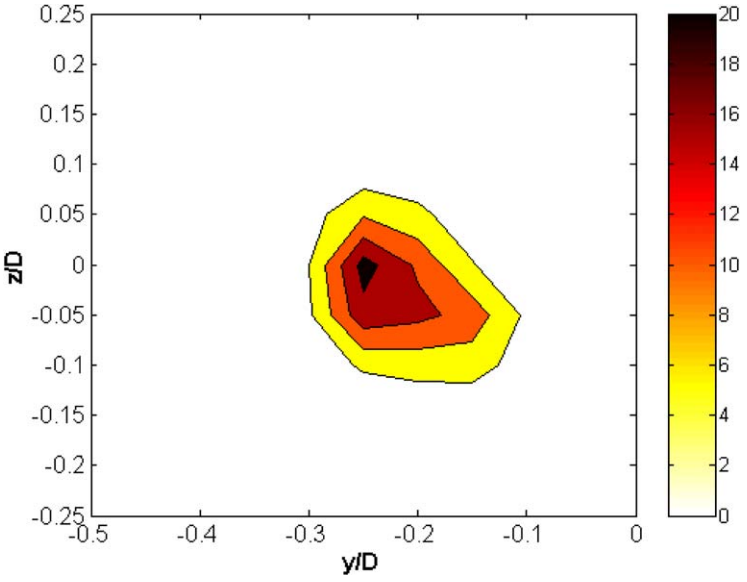

Fig. 13. Two-dimensional probability density distribution for the y- and z-component of the noise source locations for the 7 kHz broadband HTFA.

spacing between the two sources was varied between $0D$ and $6D$, while the source pair centroid was shifted from $3x/D$ to $18x/D$. Regardless of the downstream position, separations between 0 and $2D$ yielded an error less than $0.2D$, while larger separations caused an error of at most $0.5D$

(e.g., two sources centered on $9x/D$ that are separated by $6D$ had an estimated source location of $9.4x/D$). Based on this simulation, the microphone array would estimate the acoustic source for a distributed noise event as the center of the noise generating region. If the source is larger than $2D$, the array estimates the source as being between $0.2x/D$ and $0.5x/D$ downstream of the actual center of the distributed source.

These results are quite encouraging. The 3-D array was able to locate a point noise source (plasma arc) with a primary frequency that varied from 1 to 10 kHz. The plasma arc was then used as a calibration to determine the offset between the center of the 3-D array and the apparent jet centerline. The 3-D array was able to determine the area of a distributed noise source from a small fluidic device (HTFA) regardless of whether it was creating a pure acoustic tone or broadband acoustic radiation. Furthermore, distributed sources with less than a $2D$ span can be accurately located by this array, while larger sources have a small, consistent offset from the center of the distributed source. At this point, the 3-D array was deemed ready for use in determining the noise emitting region from a high-speed jet.

4. Jet noise source localization

4.1. Jet facility

The air for the high-speed jet was supplied by a four-stage compressor; it was filtered, dried, and stored in two cylindrical tanks with a total capacity of 42.5 m^3 at a pressure of 16.5 MPa (1600 ft^3 at 2500 psi). A stagnation chamber was used to condition the jet air before exhausting it through a 25.4 mm (1 in) nozzle with a lip thickness of 2.5 mm (0.1 in). The actual Mach number for the Mach 1.3 nozzle was measured as 1.28, and its Reynolds number was 1.08×10^6.

4.2. Noise source locations

A large data set was taken for noise source location analysis of the Mach 1.3 jet. The data set consists of 4.3 s of data. The data were acquired at a sampling frequency of 1 MHz with low-pass frequency filtering of 100 kHz. Based on the array's inability to accurately locate noise sources having frequencies above 10 kHz, the acoustic data was low-pass filtered at this frequency using a fifth order Chebyshev type I digital filter during post-processing. Within the 4.3 s of low-pass filtered data, there were 10,255 sound waves with a magnitude larger than 1.5σ (the standard deviation of the sound pressure level), and the apparent origin for each of these sound waves was determined. Thus, the noise source data are different from those presented in our previously published work [7–11] in that these show a three-dimensional distribution of the origins of the most intense acoustic radiation for frequencies under 10 kHz.

The x-component of the noise source locations has been plotted in the form of a probability density distribution in Fig. 14. It was created using a bin size of $1D$ with bins ranging from $-5D$ to $25D$. There were only 47 instances (out of over 10,000 noise source locations) where the array predicted a noise source upstream of the nozzle exit. This is expected as there should not be any significant sound generated upstream of the formation of the jet's shear layer and is another example of the apparent accuracy of this microphone array configuration. The mean of the

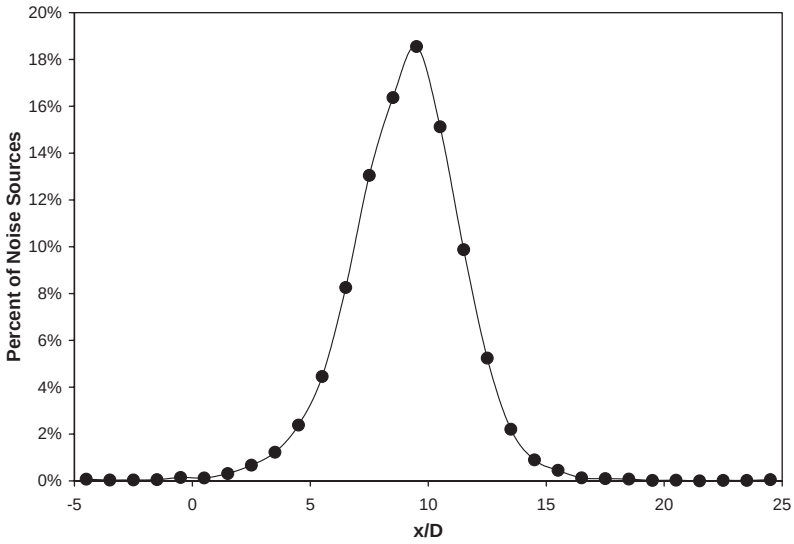

Fig. 14. Probability density distributions for the x-component of the noise source locations for the Mach 1.3 jet.

Table 1
Percent of Noise Source Locations (NSL) within different downstream ranges for the Mach 1.3 jet

Range of x-locations (D)	Percent of NSL within range
2.0 to 15.0	98
3.0 to 12.0	89
6.0 to 12.0	81
7.0 to 10.0	63

distribution was 9.0D with a standard deviation of 2.5D. Table 1 shows what percent of noise source locations were contained within various downstream ranges. Over 80% of the sound sources were located between one and two lengths of the potential core (6D to 12D).

These results differ from those obtained from the linear array of Ref. [2], which assumed a centerline distribution, lacked frequency filtering, and used a range of downstream microphone separations to determine the noise source location. For the inline array, the mean of the noise source locations was 6.7D and the standard deviation was 2.3D. The vast majority (74%) of the noise sources for the inline array were located in the region between 4D and 9D; and 98% originated between 1D and 12D. These regions can be compared to those calculated by the 3-D array between 6D and 12D (81% of calculated noise source locations), and that between 2D and 15D (98%). To reiterate, the 3-D array predicted that the noise emitting region of the jet was located farther downstream and the region covered a larger area than was predicted with the inline array.

The difference between the two distributions is due to the centerline noise source location assumption that was inherent to the inline array, the effect of frequency filtering, as well as the varied microphone spacing. If the source was on the inline array side of the jet (above the

centerline), then this assumption would cause the source to appear farther upstream than it truly was. If the source was opposite the jet centerline from the inline array (under the centerline), then the location of the source would be influenced by refraction [12]. Therefore, if the majority of the intense acoustic waves reached the array without significant refraction (they originated on the inline array side of the jet), then the distribution should appear to be farther upstream than it actually was. The inline array used six separate microphone separations to determine six noise source locations. These were then averaged to get a single source location for each acoustic event. The smaller separations yielded source locations that were generally upstream of that predicted by the wider separations thus causing an upstream shift in the mean noise source location. Additionally, higher frequency acoustic radiation originates from a region close to the jet exit [7–11]. By eliminating higher frequencies from the acoustic data prior to noise source processing, one would expect the distribution to move downstream.

The y and z distributions from the 3-D microphone array have been plotted for all of the downstream locations in the form of a 2-D probability density contour plot in Fig. 15. The bin size for the plot is $0.05D$, but the range covered in the plot is $2D$ (50.8 mm). This range is much larger than that of Figs. 11–13. The distribution is centered on the origin, which is coincident with the jet centerline. The means of the y and z distributions are both less than $0.1D$, and their standard deviations are both $0.4D$. An axisymmetric distribution that is centered on the jet centerline is expected for the round nozzle, which further confirms the accuracy of this microphone arrangement/noise location technique. In thee-dimensional space, the noise source distribution is an ellipsoid with a maximum diameter at $9x/D$. Since the region of noise generation is past the end of the potential core, it is sensible that the jet has a solid, and not a doughnut-shaped distribution of noise sources.

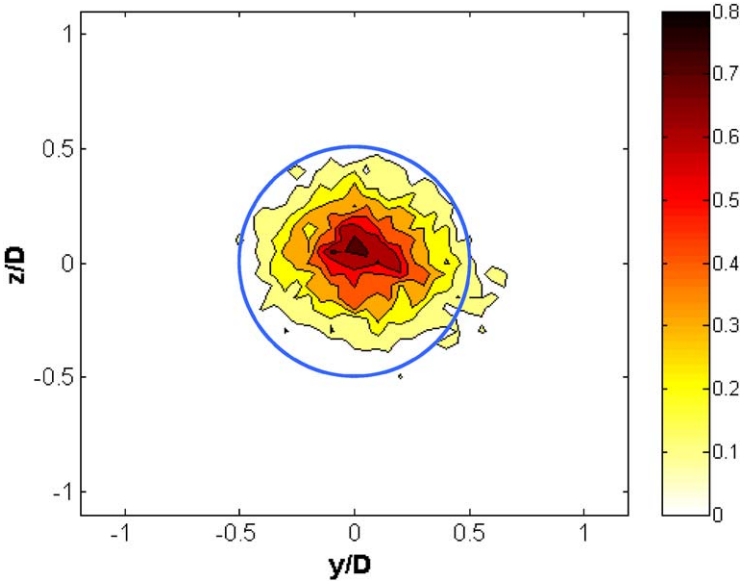

Fig. 15. Two-dimensional probability density distribution for the y- and z-component of the noise source locations for the Mach 1.3 jet.

5. Conclusion

To reduce uncertainties in the determination of noise source origins within a high-speed jet using a linear array of microphones, a 3-D microphone array was developed. The development consisted of the array hardware as well as the associated algorithm to obtain noise origins from raw microphone data. The array has an azimuthal distribution of microphones at 60° increments. There is an additional microphone placed 19.1 cm (7.5D) downstream to create inline arrays at the top and bottom of the array. The purpose of having such an arrangement is to allow the computation of all three spatial components of a noise source location using microphones that are located on the same side of the jet as the origin of the sound wave. This should reduce the impact of refraction on the predicted noise source location.

Based on a simple error analysis assuming worst case scenarios, the uncertainty in the measurement of the streamwise component of the noise source location (x-component; see Fig. 2) using this 3-D array would be $\pm 1.0D$ while that of the other two components (y- and z-component) would be negligible. Both a sinusoidally generated plasma and a high-frequency fluidic device (HTFA) were used to determine the accuracy of the 3-D array/noise source location algorithm. After a slight correction to the microphone locations (based on preliminary results), the locations were predicted accurately for frequencies up to 10 kHz.

The 3-D array was then used to analyze the noise emitting region of a Mach 1.3 jet and to compute the origin for every sound 'event' that had a magnitude larger than 1.5σ. In the streamwise direction, the vast majority (81%) of the noise sources was located between 6D and 12D and almost all (98%) of the noise sources were between 2D and 15D. Thus, over 80% of the noise origins were between one and two potential core lengths. The mean of both the y and z directions were near the jet centerline, which is expected for this axisymmetric jet. Based on these results, the 3-D array and the accompanying noise source algorithm appear to be quite accurate in predicting noise source origins from a variety of noise sources.

Acknowledgements

This work is sponsored by the Air Force Office of Scientific Research with Dr. John Schmisseur as the Technical Monitor. Many fruitful discussions on the design of the array with Dr. Satish Narayanan of UTRC are greatly appreciated. The authors would also like to acknowledge Jeffrey Kastner for the use of the HTFA and his aid in its operation, as well as Jeffrey Kastner and Edgar Caraballo for their help in the development of the noise source location codes and the conduct of the experiments. The first author would like to thank the Ohio Space Grant Consortium for his Doctoral Fellowship, and the second author would like to thank the Department of Defense for his National Defense Science and Engineering Graduate fellowship.

Appendix A. Uncertainty analysis

This appendix discusses the worst-case uncertainty analysis that was discussed in Section 2.3. The focus is on the uncertainty due to the measurement of pertinent array parameters.

The first assumption in this analysis is that the ring structure is centered on the jet centerline and the face of the ring is orthogonal to the jet centerline. The radial distance from the ring center to each microphone was measured first. The ring was designed with an inner radius of $762.00 + 0.00/-0.25$ mm ($30.00 + 0.000/-0.010$ in). The radial distance from each of the microphone diaphragms to the center of the ring was measured as 661.67 ± 0.38 mm (26.050 ± 0.015 in). The distance from the front of the ring to the center of the microphones also needed determined. The four azimuthally mounted microphones (microphones 1, 4, 5, and 8 of Fig. 2) were held into the ring by extension posts. The space between the face of the ring and the centers for these four microphones was 46.99 ± 0.51 mm (1.850 ± 0.020 in). The distance between the inline microphones and the ring face were measured as 49.33 and 50.47 mm (1.942 and 1.987 in), respectively for the top and bottom, with an assumed uncertainty of ± 0.51 mm (± 0.020 in). The inline microphones were held in an aluminum block with a separation of 190.50 ± 0.05 mm (7.500 ± 0.002 in). The azimuthal spacing in the machining of the ring was held to a tolerance of 20 s of a degree for every 10° of hole spacing. The space between the sets of mounting holes and the extension posts had minimal clearance, and as such, the azimuthal spacing was set as $60 \pm 0.1^\circ$.

The combined effect for the uncertainties of the last paragraph was determined by using a set of time separations that without any uncertainties gave a noise source location of $[216.41, 0.51, 0.00]$ mm. A maximum offset from this location was achieved with the following set of errors: 0.38 mm (0.015 in) in the radial direction, 0.51 mm (0.020 in) in the downstream direction, 0.1° azimuthal spacing and 0.05 mm (0.002 in) inline separation. For this set of errors, the worst-case scenario noise source location was [205.99, 0.25, 0.00] mm. The anechoic chamber temperature, which gives the speed of sound, was measured using an Omega handheld thermometer with a quoted uncertainty of $\pm 3.6^\circ$C ($\pm 2^\circ$F). There is ± 1 μs uncertainty in any of the time delay measurements (acquisition rate of 1 MHz). These two uncertainties can be combined with those given previously to yield a worst-case scenario noise source location of $[192.53, 0.76, 0.51]$ mm. Thus, if all of the random variations in the measurements were combined into a worst-case scenario, the noise source location would be offset by 23.9 mm (0.94 in) in the x direction and by less than a millimeter in the y and z directions. Apparently, these uncertainties have a much larger affect in the x direction calculations than in the y or z.

The errors from the second listed item are less quantifiable than the first set. This is because they are measurements made relative to the jet centerline, which in our facility, is not easily measured to the accuracy of the first set of errors. The uncertainty in the x direction placement was estimated as 3 mm (1/8 in), which can be added to the uncertainty from the previous paragraph to give a worst case uncertainty of 27 mm (1.1 in). The offset in the y and z directions was unknown. Fortunately, the y and z offsets (deviation from the ring and jet centers) were later determined by performing validations with the plasma arc and the HTFA.

References

[1] J. Hileman, M. Samimy, Turbulence structures and the acoustic far-field of a Mach 1.3 jet, *American Institute of Aeronautics and Astronautics Journal* 39 (2001) 1716–1727.

[2] J. Hileman, B. Thurow, M. Samimy, Exploring noise sources using simultaneous acoustic measurements and real-time flow visualizations in jets, *American Institute of Aeronautics and Astronautics Journal* 40 (2002) 2382–2392.

[3] C.K.W. Tam, in: H. H. Hubbard (Ed.), Jet noise generated by large-scale coherent motion, *Aeroacoustics of Flight Vehicles*: *Theory and Practice*, *Vol. 1*: *Noise Sources*, National Aeronautics and Space Administration RP 1258, W RDC TR C90-3052, 1991, pp. 311–390.
[4] G.L. Morrison, D.K. McLaughlin, Noise generation by instabilities in low Reynolds number supersonic jets, *Journal of Sound and Vibration* 65 (1979) 177–191.
[5] J.C. Yu, D.S. Dosanjh, Noise field of a supersonic Mach 1.5 cold model jet, *Journal of the Acoustical Society of America* 51 (1972) 1400–1410.
[6] M. Schaffar, Direct measurements of the correlation between axial in-jet velocity fluctuations and far-field noise near the axis of a cold jet, *Journal of Sound and Vibration* 64 (1979) 73–83.
[7] J. Simonich, S. Narayanan, T.J. Barber, M. Nishimura, Aeroacoustic characterization, noise reduction, and dimensional scaling effects of high subsonic jets, *American Institute of Aeronautics and Astronautics Journal* 39 (2001) 2062–2069.
[8] K.K. Ahuja, K.C. Massey, M.S. D'Agostino, A simple technique of locating noise sources of a jet under simulated forward motion, American Institute of Aeronautics and Astronautics Paper 98-2359, 1998.
[9] M.J. Fisher, M. Harper-Bourne, S.A.L. Glegg, Jet engine source location: the polar correlation technique, *Journal of Sound and Vibration* 51 (1977) 23–54.
[10] W.T. Chu, J. Laufer, K. Kao, Noise source distribution in subsonic jets, Inter-Noise 72, Institute of Noise Control Engineering of the USA, Washington, DC, 1972.
[11] F.R. Grosche, Distributions of sound source intensities in subsonic and supersonic jets, CP-31, AGARD Paper 4, 1973.
[12] J.B. Freund, T.G. Fleischman, Ray traces through unsteady jet turbulence, *International Journal of Aeroacoustics* 1 (2002) 83–96.
[13] J. Hileman, M. Samimy, Effects of vortex generating tabs on noise sources in an ideally expanded Mach 1.3 jet, *International Journal of Aeroacoustics* 2 (1) (2003) 35–63.
[14] K.K. Ahuja, H.K. Tanna, B.J. Tester, An experimental study of transmission, reflection and scattering of sound in a free jet flight simulation facility and comparison with theory, *Journal of Sound and Vibration* 75 (1981) 51–85.
[15] C.W. Kerechanin, M. Samimy, J.-H. Kim, Effects of nozzle trailing edges on acoustic field of supersonic rectangular jet, *American Institute of Aeronautics and Astronautics Journal* 39 (2001) 1065–1070.
[16] J. Kastner, M. Samimy, Development and characterization of Hartmann tube based fluidic actuators for high-speed flow control, *American Institute of Aeronautics and Astronautics Journal* 40 (2002) 1926–1934.
[17] J. Kastner, A Study of the Hartman Tube for its Development and Use as an Actuator in High Speed Flow Control, MS Thesis, The Ohio State University, 2002.
[18] G. Raman, V. Kibens, A. Cain, J. Lepicovsky, Advanced actuator concepts for active aeroacoustic control, American Institute of Aeronautics and Astronautics Paper 2000-1930, 2000.
[19] J. Hileman, B. Thurow, M. Samimy, Acoustic source localization using a 3-D microphone array in a Mach 1.3 jet, American Institute of Aeronautics and Astronautics Paper 2002-0366, 2002.
[20] J. Hartmann, B. Trolle, A new acoustic generator: the air-jet generator, *Journal of Scientific Instruments* 4 (1927) 101–111.